CERN-TH-2020-147, JLAB-THY-20-3242

Supplementary material for: The energy-dependent $\pi^+\pi^+\pi^+$ scattering amplitude from QCD

Maxwell T. Hansen,[1,*] Raul A. Briceño,[2,3,†] Robert G. Edwards,[2,‡] Christopher E. Thomas,[4,§] and David J. Wilson[4,¶]

(for the Hadron Spectrum Collaboration)

[1] *Theoretical Physics Department, CERN, 1211 Geneva 23, Switzerland*
[2] *Thomas Jefferson National Accelerator Facility, 12000 Jefferson Avenue, Newport News, VA 23606, USA*
[3] *Department of Physics, Old Dominion University, Norfolk, VA 23529, USA*
[4] *DAMTP, University of Cambridge, Wilberforce Road, Cambridge, CB3 0WA, UK*

(Dated: October 8, 2020)

CONTENTS

* maxwell.hansen@cern.ch
† rbriceno@jlab.org
‡ edwards@jlab.org
§ c.e.thomas@damtp.cam.ac.uk
¶ d.j.wilson@damtp.cam.ac.uk

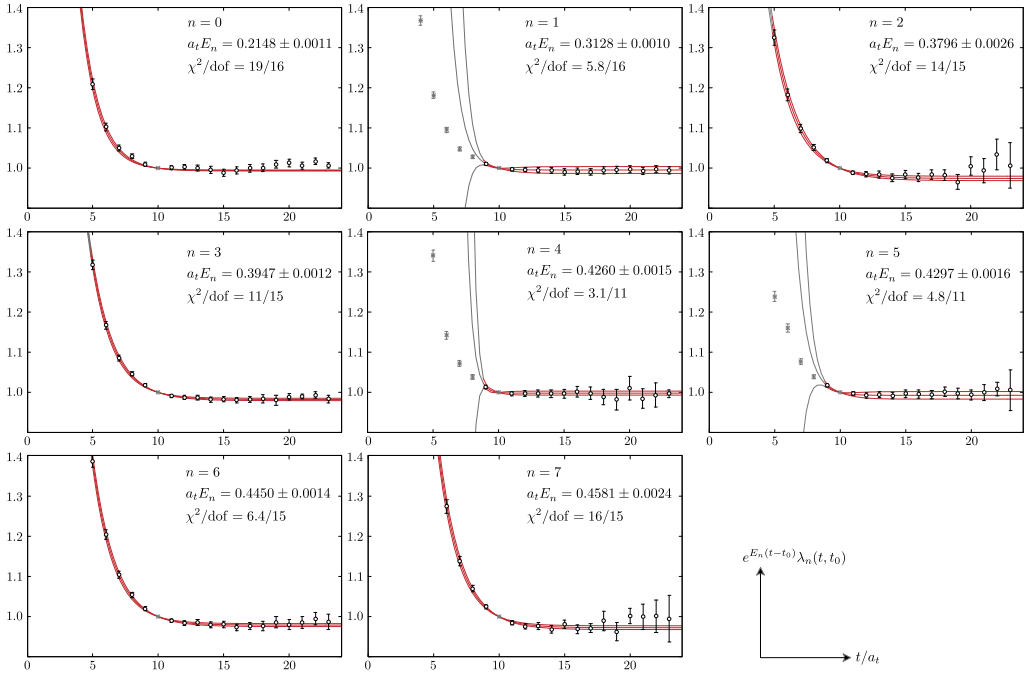

FIG. 1. GEVP eigenvalues used to determine the $\boldsymbol{P} = [000]$, $\Lambda = A_1^-$, three-pion spectrum on the $20^3 \times 256$ ensemble. As explained in the text, the diagonalization is performed with $t_0/a_t = 10$ and the eigenvalues are rescaled by their expected large-t fall-off.

1. Spectra

In this section we give details concerning the finite-volume spectra described in the main text. We focus here on two representative examples for the correlators used to extract the three-pion energies. The quality of two-pion correlators can be inferred from the earlier work presented in Ref. [1], which includes a partially overlapping data set.

As a first example, consider the three-pion spectrum for the $\boldsymbol{P} = [000]$, $\Lambda = A_1^-$ irrep on the $20^3 \times 256$ ensemble. In this case $G_{ij}(t) = \langle \mathcal{O}_i(t) \mathcal{O}_j^\dagger(0) \rangle$ is an 8×8 matrix of correlators, built from the first 8 operators listed in Table VI of Sec. 5. In Fig. 1 we plot the corresponding eigenvalues, $\lambda_n(t, t_0)$, of the matrix

$$M(t, t_0) \equiv G(t_0)^{-1/2} \cdot G(t) \cdot G(t_0)^{-1/2} \,, \tag{1}$$

entering the generalized eigenvalue problem (GEVP). These are determined for $t_0/a_t = 10$ and are plotted vs. t/a_t for a range of values both before and after the reference time. To display the eigenvalues in a useful manner, we plot the combination $e^{E_n(t-t_0)}\lambda_n(t, t_0)$, where E_n has been determined from a two-state fit to $\lambda_n(t, t_0)$

$$\lambda_n(t, t_0) = (1 - A_n) e^{-E_n(t-t_0)} + A_n e^{-E'_n(t-t_0)} \,. \tag{2}$$

The quality of the fit is indicated by the χ^2/dof in each panel. The plotted combination behaves as expected for a successful GEVP, showing a reasonable plateaux over a range of t/a_t.

This result also exhibits no evidence for thermal states on this lattice, as expected given the length of the temporal extent, $m_\pi T \approx 17.7$. We detour slightly, to explain this point in more detail:

In general, for multi-pion systems, the leading finite-T effects are given by

$$G_{ij}(t) = \langle 0 | \mathcal{O}_i(0)\, e^{-\hat{H}t}\, \mathcal{O}_j^\dagger(0) | 0 \rangle + e^{-m_\pi(T-t)} \langle \pi^- | \mathcal{O}_i(0)\, e^{-\hat{H}t}\, \mathcal{O}_j^\dagger(0) | \pi^- \rangle + \cdots \,, \tag{3}$$

where $\hat{H}$ is the Hamiltonian and the ellipsis represents thermal effects falling faster than $e^{-m_\pi T}$. For concreteness, we have assumed that $O^\dagger(0)$ creates three-π^+ quantum numbers, so that $\mathcal{O}^\dagger(0)|\pi^-\rangle$ has the quantum numbers of two pions with isospin two. A spectral decomposition of Eq. (3) then yields

$$G_{ij}(t) = \sum_n c_i^{(n)} c_j^{(n)*} e^{-E_n^{\pi\pi\pi\pi} t} + e^{-m_\pi(T-t)} \sum_n b_i^{(n)} b_j^{(n)*} e^{-E_n^{\pi\pi} t} + \cdots \,, \tag{4}$$

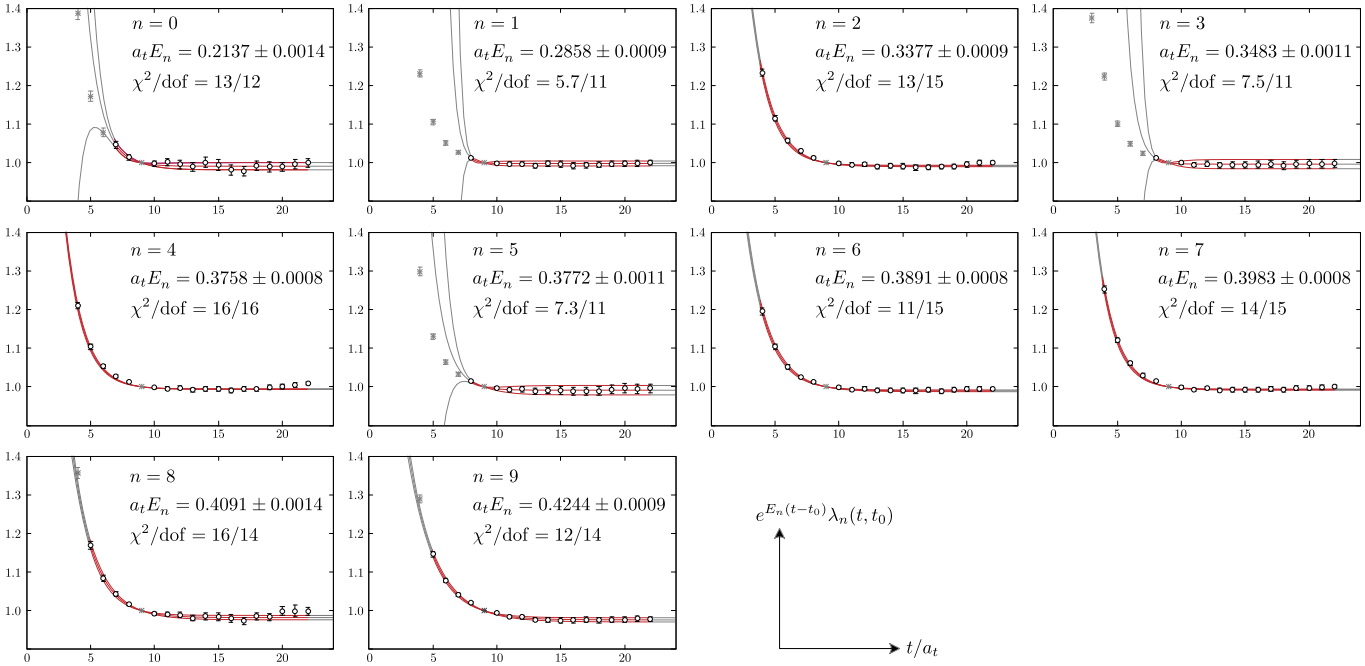

FIG. 2. GEVP eigenvalues used to determine the $\boldsymbol{P} = [000]$, $\Lambda = A_1^-$, three-pion spectrum on the $24^3 \times 128$ ensemble. The diagonalization is performed with $t_0/a_t = 9$ and the eigenvalues are rescaled as in Fig. 1.

where the sum in the first term (second term) runs over all maximal-isospin three-pion (two-pion) finite-volume states with specified $\boldsymbol{P}$. In the case of $\boldsymbol{P} = [000]$, the two- and three-pion ground states take the form $Nm_\pi + \Delta E_N$ where $N = 2, 3$ and $\Delta E_N \sim 1/L^3$ for weakly-interacting systems. Taking the leading ($n = 0$) terms of Eq. (4) and substituting this scaling then yields

$$G_{ij}(t) = c_i^{(0)} c_j^{(0)*} e^{-(3m_\pi + \Delta E_3)t} + b_i^{(0)} b_j^{(0)*} e^{-m_\pi(T+t)} e^{-\Delta E_2 t} + \cdots . \tag{5}$$

When this same exercise is performed for a *two-pion* correlator, again focusing on the case of $\boldsymbol{P} = [000]$, one finds that the leading thermal contamination is a constant in t in the non-interacting limit. As discussed in Ref. [1] this can thus be removed by applying a shift to the correlator $G_{ij}(t) \to G_{ij}(t) - G_{ij}(t + \delta t)$. In the present case, however, the leading contaminations are t-dependent. One option is to reweight and shift, i.e.

$$G_{ij}(t) \;\to\; e^{-m_\pi t}\big(G_{ij}(t)e^{m_\pi t} - G_{ij}(t+\delta t)e^{m_\pi(t+\delta t)}\big) . \tag{6}$$

This approach, already used in Ref. [1] for $\pi\pi$ systems with non-zero total momentum, reduces thermal effects at the cost of generally degrading the signal quality. Fortunately, for the $20^3 \times 256$ lattice, this is not required. Comparing the leading and subleading terms of Eq. (5), and neglecting the interactions, one finds that the relative size of the three-pion thermal contamination is $e^{-m_\pi(T-2t)}$. Thus, assuming that the relevant matrix elements have the same order of magnitude, for the range of t considered these effects are $\sim 10^{-7}$ and are safely negligible, despite the high statistical precision of the extracted energies. This concludes our general comments on thermal effects.

As a second example, in Fig. 2 we consider the same three-pion quantum numbers ($\boldsymbol{P} = [000]$, $\Lambda = A_1^-$) on the $24^3 \times 128$ ensemble. Because the larger spatial volume lowers the value of the nth level, here we include 2 additional operators to better absorb the excited states. As with the previous example, the χ^2/dof and the plotted curves provide strong evidence of a successful GEVP extraction. For this case, $e^{-m_\pi(T-2t)} \sim 10^{-3}$ so that finite-T effects potentially present a more significant issue. As a result we have also considered shifting and reweighting, as summarized by Eq. (6), in our various fits. However, across all values of $\boldsymbol{P}$, we find that more stable fits are achieved via the unmodified correlators, relying on the basis of operators to push the extraction to earlier times and examining the resulting GEVP eigenvalues. This is in contrast to the $24^3 \times 128$ two-pion fits, where the extractions are improved by shifting in certain cases, as described in Ref. [1].

2. K-matrix fits

In this subsection we give additional details concerning the K-matrix fits, summarized in the main text. We present four basic types of fits:

1. Fitting only the $\pi^+\pi^+$ spectra to various choices of $p\cot\delta(p)$ [Table I].
2. Fitting only the $\pi^+\pi^+\pi^+$ spectra to various choices of $p\cot\delta(p)$, with $\mathcal{K}_{3,\mathsf{iso}} = 0$ [Table II].
3. Fitting only the $\pi^+\pi^+\pi^+$ spectra to various choices of $\mathcal{K}_{3,\mathsf{iso}}$, with $p\cot\delta(p)$ fixed by independent $\pi^+\pi^+$ fits [Table III].
4. Fitting all spectra simultaneously to various choices of $p\cot\delta(p)$ and $\mathcal{K}_{3,\mathsf{iso}}$ [Table IV].

Here $\delta(p)$ is the S-wave, $\pi^+\pi^+$ scattering phase shift, related to the scattering amplitude via

$$\mathcal{M}_2(E_2^\star) = \frac{16\pi E_2^\star}{p\cot\delta(p) - ip}\,, \tag{7}$$

where $p^2 = E_2^{\star 2}/4 - m_\pi^2$. One standard parametrization of the scattering amplitude follows from the effective range expansion

$$p\cot\delta(p) = -\frac{1}{a_0} + \frac{1}{2}r_0 p^2 + \mathcal{O}(p^4)\,, \tag{8}$$

and below we present fits to the leading term as well as to the leading two terms.

In the case of $\pi^+\pi^+$ scattering, chiral perturbation theory predicts the Adler zero, which leads to a pole in $p\cot\delta(p)$, limiting the range of convergence for the effective range expansion. This motivates the alternative form

$$p\cot\delta(p) = A(c,p)\Big[-\frac{1}{a_0} + c' p^2 + \mathcal{O}(p^4)\Big]\,, \tag{9}$$

where we have introduced

$$A(c,p) \equiv \frac{c\, m_\pi \sqrt{p^2 + m_\pi^2}}{2p^2 + c\, m_\pi^2}\,. \tag{10}$$

The function $A(c,p)$ is chosen to match the analytic structure predicted by leading-order chiral perturbation theory (both the energy numerator and the pole in the denominator) and is normalized so that $A(c,0) = 1$. The leading-order prediction for the pole position corresponds to $c = 1$ and in the following we present fits both with c fixed and allowed to vary.

As we explain in detail in Sec. 3 below, the three-particle scattering amplitude, $\mathcal{M}_3$, is determined from the two-particle scattering amplitude together with a local three-particle K matrix, first introduced in Ref. [2] and denoted by $\mathcal{K}_{\mathrm{df},3}$. As already described in the main text, we work here in the isotropic approximation, for which this three-particle K matrix reduces to a simple function of the total center-of-momentum frame energy, denoted $\mathcal{K}_{3,\mathsf{iso}}(E_3^\star)$. This quantity admits an expansion similar to the effective range expansion

$$\mathcal{K}_{3,\mathsf{iso}}(E_3^\star) = c_1/m_\pi^2 + c_2\Delta/m_\pi^4 + \mathcal{O}(\Delta^2)\,, \tag{11}$$

where $\Delta \equiv E_3^{\star 2} - 9m_\pi^2$. The fits presented below take either the first or else the first two terms in this expansion.

In each case, the fit is performed by minimizing the $\chi^2(\{\eta_i\})$, where

$$\chi^2(\{\eta_i\}) \equiv [\boldsymbol{\mathcal{E}}_{\mathsf{d}} - \boldsymbol{\mathcal{E}}(\{\eta_i\})]\cdot C^{-1}\cdot[\boldsymbol{\mathcal{E}}_{\mathsf{d}} - \boldsymbol{\mathcal{E}}(\{\eta_i\})]^{\mathrm{T}}\,. \tag{12}$$

Here $\boldsymbol{\mathcal{E}}_{\mathsf{d}}$ is a vector built from two and three-particle energies extracted from the lattice calculation, C is the covariance matrix, and $\boldsymbol{\mathcal{E}}(\{\eta_i\})$ is a vector of solutions to the two- and three-particle quantization conditions. The solved energies depend on $\{\eta_i\}$, which stands for all two- and three-particle K-matrix parameters, over which the minimization is performed.

In certain cases the low-lying eigenvalues of C cannot be estimated reliably and, if underestimated, can lead to artificially enhanced eigenvalues in C^{-1}, and therefore inflated values for $\chi^2(\{\eta_i\})$. To study this problem we have also

Fit	$E^\star_{2,\mathrm{cut}}$	$p\cot\delta(p)$	fit result	χ^2/dof
A_2	$4.0m_\pi$	$-1/a_0$	$m_\pi a_0 = 0.278 \pm 0.007$	$89.8/(32-1) = 2.90$
B_2	$3.4m_\pi$	$-1/a_0$	$m_\pi a_0 = 0.292 \pm 0.010$	$26.9/(21-1) = 1.35$
C_2	$4.0m_\pi$	$-1/a_0 + r_0p^2/2$	$m_\pi a_0 = 0.317 \pm 0.015$ $\begin{bmatrix}1.0 & -0.9\\ & 1.0\end{bmatrix}$ $m_\pi r_0 = -0.39 \pm 0.12$	$79.6/(32-2) = 2.65$
D_2	$3.4m_\pi$	$-1/a_0 + r_0p^2/2$	$m_\pi a_0 = 0.258 \pm 0.018$ $\begin{bmatrix}1.0 & -0.9\\ & 1.0\end{bmatrix}$ $m_\pi r_0 = 0.68 \pm 0.33$	$22.7/(21-2) = 1.20$
E_2	$4.0m_\pi$	$-A(c_0,p)/a_0$	$m_\pi a_0 = 0.355 \pm 0.021$ $\begin{bmatrix}1.0 & -0.8\\ & 1.0\end{bmatrix}$ $m_\pi c_0 = 11.2 \pm 2.1$	$96.7/(32-2) = 3.22$
F_2	$3.4m_\pi$	$-A(c_0,p)/a_0$	$m_\pi a_0 = 0.260 \pm 0.035$ $\begin{bmatrix}1.0 & -0.9\\ & 1.0\end{bmatrix}$ $m_\pi c_0 = 3.7 \pm 1.1$	$22.7/(21-2) = 1.20$
G_2	$4.0m_\pi$	$A(1,p)(-1/a_0 + c_0p^2)$	$m_\pi a_0 = 0.223 \pm 0.019$ $\begin{bmatrix}1.0 & 0.9\\ & 1.0\end{bmatrix}$ $m_\pi c_0 = -2.88 \pm 0.19$	$70.1/(32-2) = 2.34$
H_2	$3.4m_\pi$	$A(1,p)(-1/a_0 + c_0p^2)$	$m_\pi a_0 = 0.184 \pm 0.022$ $\begin{bmatrix}1.0 & 0.96\\ & 1.0\end{bmatrix}$ $m_\pi c_0 = -2.2 \pm 0.4$	$26.5/(21-2) = 1.40$
I_2 $[r = 0.01\ (9/32)]$	$4.0m_\pi$	$-1/a_0$	$m_\pi a_0 = 0.292 \pm 0.008$	$40.5/(32-1) = 1.31$
J_2 $[r = 0.01\ (9/32)]$	$4.0m_\pi$	$-1/a_0 + r_0p^2/2$	$m_\pi a_0 = 0.300 \pm 0.016$ $\begin{bmatrix}1.0 & -0.8\\ & 1.0\end{bmatrix}$ $m_\pi r_0 = -0.08 \pm 0.14$	$40.3/(32-2) = 1.34$

TABLE I. Summary of fits to $\pi^+\pi^+$ finite-volume energies, for various choices of $p\cot\delta(p)$. All values of total momentum $\boldsymbol{P}$ (from [000] to [002]) and both volumes (20^3 and 24^3) are used in each fit. The entries below the lower double horizontal line are determined using a regularized covariance matrix as explained in the text. The function $A(c_0,p) = c_0 m_\pi \sqrt{p^2+m_\pi^2}/(2p^2+c_0m_\pi^2)$ encodes the effect of the Adler zero, with $c_0 = 1$ corresponding to the pole position from leading-order chiral perturbation theory. The columns are understood as follows: "Fit" gives a label to the fit (and defines the regularized covariance matrix for the final two fits); "$E^\star_{2,\mathrm{cut}}$" gives the two-particle center-of-momentum frame energy cutoff (i.e. only points with central values below this threshold enter the fit); "$p\cot\delta(p)$" indicates the fit function; "fit result" displays the extracted parameters and their correlation; "χ^2/dof" gives the value of $\chi^2(\{\eta_i\})$ (evaluated at the best fit parameters) divided by the number of degrees of freedom.

considered an alternative method in which the low lying eigenvalues of C are adjusted. To do so, one first diagonalizes C

$$C = R^{\mathrm{T}} \cdot D \cdot R\,, \tag{13}$$

where R is an orthogonal matrix of eigenvectors and D a diagonal matrix of eigenvalues. We label the eigenvalues (ordered from smallest to largest) by $\lambda_1, \cdots, \lambda_N$ and note that these are positive. We assume also that the rows and columns of R are organized such that

$$D = \mathrm{diag}[\lambda_1, \lambda_2, \cdots, \lambda_N]\,. \tag{14}$$

$\chi^2(\{\eta_i\})$ may be poorly estimated if there is a large hierarchy between the smallest and largest eigenvalues, λ_1 and λ_N, respectively. This motivates the definition

$$C_r = R^{\mathrm{T}} \cdot D_r \cdot R\,, \tag{15}$$

where D_r is a diagonal matrix defined as

$$D_r = \mathrm{diag}\Big[\max[\lambda_1, r\lambda_N],\ \max[\lambda_2, r\lambda_N],\ \cdots,\ \max[\lambda_N, r\lambda_N]\Big]\,. \tag{16}$$

Note, if $r = 0$, then $D = D_r \implies C = C_r$. As this parameter is increased, the lowest eigenvalues are adjusted to some fixed fraction of the largest value. This approach defines a new test statistic and, in principle, one can sample its corresponding distribution to define p-values and assess the quality of fits. This goes beyond the scope of this work and we only perform the modified fits as a cross check to show that the extracted fit parameters are robust under

these regularizations of the covariance matrix. Such fits are reported in the tables of this section with labels of the form $[r = 0.01\ (n/m)]$ where r indicates the adjustment parameter and (n/m) indicates the number of eigenvalues that have been changed versus the total number. We have additionally re-done many of the fits summarized Tables I-IV with the pion mass, m_π, and the anisotropy, ξ, varied by one standard deviation. We find in all cases that the effect of this shift is well below the statistical uncertainties on the extracted fit parameters.

Fit	$E^\star_{3,\text{cut}}$	$p\cot\delta(p)$	fit result	χ^2/dof
$\text{A}_{3(\text{K2})}$	$4.4m_\pi$	$-1/a_0$	$m_\pi a_0 = 0.293 \pm 0.011$	$31.5/(16-1) = 2.10$
$\text{B}_{3(\text{K2})}$ $[r = 0.01\ (5/16)]$	$4.4m_\pi$	$-1/a_0$	$m_\pi a_0 = 0.298 \pm 0.014$	$24.5/(16-1) = 1.63$

TABLE II. Summary of fits to $\pi^+\pi^+\pi^+$ finite-volume energies, for $p\cot\delta(p) = -1/a_0$ with $\mathcal{K}_{3,\text{iso}} = 0$ fixed. All values of total momentum $\boldsymbol{P}$ (from [000] to [111]) and both volumes (20^3 and 24^3) are used in each fit. Columns as in Table I, with "$E^\star_{3,\text{cut}}$" indicating the three-particle center-of-momentum frame energy cutoff.

Fit	$p\cot\delta(p)$	$E^\star_{3,\text{cut}}$	$\mathcal{K}_{3,\text{iso}}$	fit result	χ^2/dof
$\text{A}_{3(\text{K3})}$	$-1/a_0$ (B_2)	$4.4m_\pi$	c_1/m_π^2	$c_1 = -253 \pm 874$	$31.4/(16-1) = 2.10$
$\text{B}_{3(\text{K3})}$	$-1/a_0$ (B_2)	$4.4m_\pi$	$c_1/m_\pi^2 + c_2\Delta/m_\pi^4$	$c_1 = 5039 \pm 1731$ $\begin{bmatrix}1.0 & -0.8\\ & 1.0\end{bmatrix}$ $c_2 = -637 \pm 92$	$25.9/(16-2) = 1.85$
$\text{C}_{3(\text{K3})}$ $[r = 0.01\ (5/16)]$	$-1/a_0$ (B_2)	$4.4m_\pi$	c_1/m_π^2	$c_1 = -524 \pm 892$	$24.4/(16-1) = 1.63$

TABLE III. Summary of fits to $\pi^+\pi^+\pi^+$ finite-volume energies, for various choices of $\mathcal{K}_{3,\text{iso}}$ (with $p\cot\delta(p)$ given by fit B_2 of Table I). Columns as in Tables I and II, with "$\mathcal{K}_{3,\text{iso}}$" indicating the fit function used and $\Delta \equiv E_3^{\star 2} - 9m_\pi^2$ encoding a linear-dependence in the squared center-of-momentum frame energy.

Fit	$E^\star_{2,\text{cut}}$	$E^\star_{3,\text{cut}}$	$p\cot\delta(p)$	$\mathcal{K}_{3,\text{iso}}$	fit result	χ^2/dof
A_{2+3}	$3.4m_\pi$	$4.4m_\pi$	$-1/a_0$	0	$m_\pi a_0 = 0.300 \pm 0.007$	$64.7/(37-1) = 1.80$
B_{2+3}	$3.4m_\pi$	$4.4m_\pi$	$-1/a_0$	c_1/m_π^2	$m_\pi a_0 = 0.296 \pm 0.008$ $\begin{bmatrix}1.0 & 0.6\\ & 1.0\end{bmatrix}$ $c_1 = -339 \pm 770$	$64.5/(37-2) = 1.84$
C_{2+3} $[r = 0.005\ (11/37)]$	$3.4m_\pi$	$4.4m_\pi$	$-1/a_0$	0	$m_\pi a_0 = 0.297 \pm 0.008$	$50.9/(37-1) = 1.42$
D_{2+3} $[r = 0.005\ (11/37)]$	$3.4m_\pi$	$4.4m_\pi$	$-1/a_0$	c_1/m_π^2	$m_\pi a_0 = 0.293 \pm 0.010$ $\begin{bmatrix}1.0 & 0.7\\ & 1.0\end{bmatrix}$ $c_1 = -426 \pm 814$	$50.7/(37-2) = 1.45$

TABLE IV. Summary of combined fits to both two- and three-pion energies. Columns as in Tables I-III.

3. Details of the three-particle integral equations

In this subsection we give additional details concerning Eq. (5) of the main text and give details on its numerical implementation. We begin by reviewing the integral equations presented in Ref. [3]. As the results of the fits summarized in the main text (and detailed in the previous subsection) are consistent with $\mathcal{K}_{3,\text{iso}} = 0$, we focus here on the case of a weak three-body interaction, keeping only the linear contribution in this term. We begin with the unsymmetrized three-body scattering amplitude

$$\mathcal{M}_3^{(u,u)}(\boldsymbol{p},\boldsymbol{k}) = \mathcal{D}^{(u,u)}(\boldsymbol{p},\boldsymbol{k}) + \mathcal{E}^{(u)}(\boldsymbol{p})\mathcal{K}_{3,\text{iso}}\mathcal{E}^{(u)}(\boldsymbol{k}) + \mathcal{O}(\mathcal{K}_{3,\text{iso}}^2)\,, \tag{17}$$

where the superscripts indicate the lack of exchange symmetry, and $\boldsymbol{k}$ and $\boldsymbol{p}$ specify the momenta of the so-called spectator particles in the initial and final state, respectively. In general, the factors appearing in Eq. (17) carry angular momentum indices. However, as discussed in the main text, the $\pi^+\pi^+$ system at low energies is dominated by the S-wave component. Thus, we restrict attention here to $\pi^+\pi^+$ with zero angular momentum, such that $\mathcal{M}_3^{(u,u)}(\boldsymbol{p},\boldsymbol{k})$ and $\mathcal{D}^{(u,u)}(\boldsymbol{p},\boldsymbol{k})$ are simple functions, with no implicit indices.

In this limiting case, $\mathcal{D}^{(u,u)}(\boldsymbol{p},\boldsymbol{k})$ satisfies the implicit equation

$$\mathcal{D}^{(u,u)}(\boldsymbol{p},\boldsymbol{k}) = -\mathcal{M}_2(E^\star_{2,p})G^\infty(\boldsymbol{p},\boldsymbol{k})\mathcal{M}_2(E^\star_{2,k}) - \mathcal{M}_2(E^\star_{2,p})\int \frac{d^3\boldsymbol{k}'}{(2\pi)^3 2\omega_{k'}} G^\infty(\boldsymbol{p},\boldsymbol{k}')\mathcal{D}^{(u,u)}(\boldsymbol{k}',\boldsymbol{k})\,, \tag{18}$$

where $E^{\star 2}_{2,k} \equiv (E-\omega_k)^2 - k^2$ is the center-of-momentum energy for the non-spectator pair (with $k = |\boldsymbol{k}|$ defined in the three-particle zero-momentum frame). In words, the unsymmetrized amplitude $\mathcal{D}^{(u,u)}$ can be evaluated by solving an integral equation depending only on the two-particle scattering amplitude $\mathcal{M}_2(E^\star_{2,p})$ and the exchange propagator

$$G^\infty(\boldsymbol{p},\boldsymbol{k}) \equiv \frac{H(p,k)}{b_{pk}^2 - m^2 + i\epsilon}\,. \tag{19}$$

Here we have suppressed the π subscript on the mass and have introduced $b^2_{pk} \equiv (E^\star - \omega_p - \omega_k)^2 - (\boldsymbol{p}+\boldsymbol{k})^2$ as well as $H(p,k)$, a cut-off function built into the relation between finite-volume energies and $\mathcal{K}_{3,\mathsf{iso}}$, as well as that between $\mathcal{K}_{3,\mathsf{iso}}$ and the physical scattering amplitude. The definition used here is

$$H(p,k) \equiv J\big(E^{\star 2}_{2,k}/[2m]^2\big)\,J\big(E^{\star 2}_{2,p}/[2m]^2\big)\,, \qquad J(x) \equiv \begin{cases} 0\,, & x \le 0\,; \\ \exp\left(-\frac{1}{x}\exp\left[-\frac{1}{1-x}\right]\right)\,, & 0 < x \le 1\,; \\ 1\,, & 1 < x\,. \end{cases} \tag{20}$$

(See also Refs. [2, 3] for more discussion on this technical aspect.) Finally $\mathcal{E}^{(u)}(\boldsymbol{p})$ is a function closely related to $\mathcal{D}^{(u,u)}(\boldsymbol{p},\boldsymbol{k})$ and defined, in a specific limiting case, in Eq. (28) below. In this work it is only relevant to demonstrate that $\mathcal{K}_{3,\mathsf{iso}}$ contributes negligibly to both the central value and uncertainty of the three-hadron scattering amplitude, as we describe in the following section.

The next step is to project the remaining directional freedom within $\mathcal{D}^{(u,u)}$ onto vanishing three-particle angular momentum, i.e. to $J = 0$. Defining

$$\mathcal{D}_{\mathsf{s}}^{(u,u)}(p,k) \equiv \int \frac{d\Omega_{\hat{k}}}{4\pi}\frac{d\Omega_{\hat{p}}}{4\pi}\mathcal{D}^{(u,u)}(\boldsymbol{p},\boldsymbol{k})\,, \tag{21}$$

one can show that $\mathcal{D}_{\mathsf{s}}$ satisfies a one-dimensional integral equation of the form

$$\mathcal{D}_{\mathsf{s}}^{(u,u)}(p,k) = -\mathcal{M}_2(E^\star_{2,p})G_{\mathsf{s}}(p,k,\epsilon)\mathcal{M}_2(E^\star_{2,k}) - \mathcal{M}_2(E^\star_{2,p})\int_0^{k_{\mathsf{max}}} \frac{k'^2\,dk'}{(2\pi)^2\omega_{k'}}\,G_{\mathsf{s}}(p,k',\epsilon)\mathcal{D}_{\mathsf{s}}^{(u,u)}(k',k), \tag{22}$$

where

$$G_{\mathsf{s}}(p,k,\epsilon) \equiv \int \frac{d\Omega_{\hat{p}}}{4\pi}\frac{d\Omega_{\hat{k}}}{4\pi}G^\infty(\boldsymbol{p},\boldsymbol{k}) = -\frac{H(p,k)}{4pk}\log\left[\frac{2pk - (E-\omega_k-\omega_p)^2 + p^2 + k^2 + m^2 - i\epsilon}{-2pk - (E-\omega_k-\omega_p)^2 + p^2 + k^2 + m^2 - i\epsilon}\right]. \tag{23}$$

In Fig. 3 we plot G_{s} for a range of kinematic values. Setting $\mathcal{K}_{3,\mathsf{iso}} = 0$ and combining Eqs. (17), (22) and (23), we arrive at Eq. (5) of the main text. Note that, in Eq. (22), we have included an explicit cutoff at $k_{\mathsf{max}} = (s+m^2)/(2\sqrt{s})$. This is done without any additional approximation as $H(p,k)$ has vanishing support for $k > k_{\mathsf{max}}$.

We comment here that, in general, projecting $\mathcal{M}_3^{(u,u)}$ to definite partial waves is not equivalent to doing the same for the symmetrized three-hadron scattering amplitude. However, as discussed around Eqs. (15) and (16) of Ref. [4] any definite-angular-momentum component of the the fully symmetric $\mathcal{M}_3$ can be assembled from known combinations of the various angular-momentum components of $\mathcal{M}_3^{(u,u)}$. Thus the latter form a basis for constructing the physical three-hadron amplitudes.

To solve Eq. (22) numerically we replace the integral $\int_0^{k_{\mathsf{max}}} dk'$ with a discrete sum $\sum_{k'} \Delta k$ containing N terms. Then a discretized version of the equation can be written in a matrix form

$$\boldsymbol{D}(N,\epsilon) = -\boldsymbol{\mathcal{M}}\cdot\boldsymbol{G}(\epsilon)\cdot\boldsymbol{\mathcal{M}} - \boldsymbol{\mathcal{M}}\cdot\boldsymbol{G}(\epsilon)\cdot\boldsymbol{P}\cdot\boldsymbol{D}(N,\epsilon)\,, \tag{24}$$

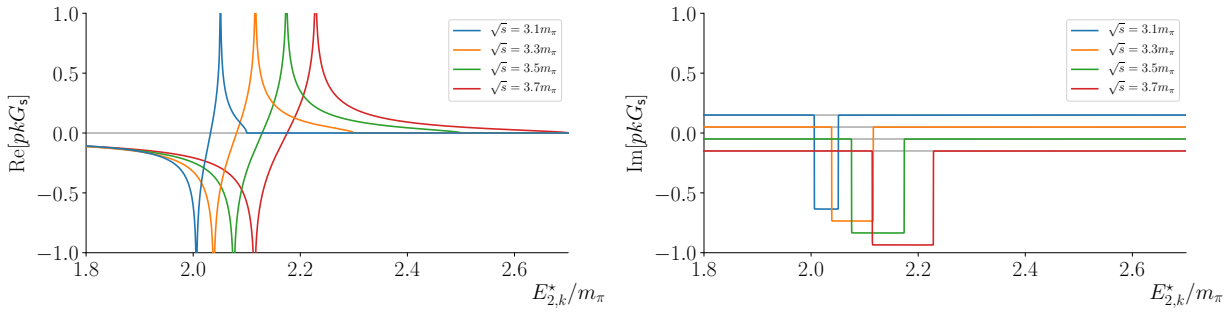

FIG. 3. Plots of the kernel function $G_\mathsf{s}(p,k,\epsilon)$ [defined Eq. (23)] vs $E^\star_{2,k}$, here for four different energies as shown in the legend and with $p = 0.1m_\pi$ and $\epsilon \to 0^+$. For $\mathrm{Im}[p\,k\,G_\mathsf{s}(p,k,\epsilon)]$, in the right panel, we have vertically off-set the curves for improved readability.

where we have introduced the following $N \times N$ matrix representations

$$\boldsymbol{G}_{pk}(\epsilon) = G_\mathsf{s}(p,k,\epsilon)\,, \qquad \boldsymbol{\mathcal{M}}_{k'k} = \delta_{k'k}\,\mathcal{M}_2(E^\star_{2,k})\,, \qquad \boldsymbol{P}_{k'k} = \delta_{k'k}\,\frac{k^2\Delta k}{(2\pi)^2\omega_k}\,, \tag{25}$$

as well as $\boldsymbol{D}(N,\epsilon)$, which becomes our target quantity in the ordered double limit

$$\mathcal{D}^{(u,u)}_\mathsf{s}(p,k) = \lim_{\epsilon\to 0}\lim_{N\to\infty} \boldsymbol{D}_{pk}(N,\epsilon)\,. \tag{26}$$

Here, in a slight abuse of notation, the indices $p\,k$ represent the choices that are closest to physical momenta p and k for a given N value. Eq. (24) can then be solved through a matrix inverse to yield

$$\boldsymbol{D}(N,\epsilon) = -\big[\mathbb{I} + \boldsymbol{\mathcal{M}}\cdot\boldsymbol{G}(\epsilon)\cdot\boldsymbol{P}\big]^{-1}\cdot\boldsymbol{\mathcal{M}}\cdot\boldsymbol{G}(\epsilon)\cdot\boldsymbol{\mathcal{M}}\,. \tag{27}$$

Finally we return to the endcap factors appearing on either side of $\mathcal{K}_{3,\mathsf{iso}}$ in Eq. (17). These are defined in Eqs. (105) and (106) of Ref. [2] and in the overall S-wave approximation they take the form

$$\mathcal{E}^{(u)}_\mathsf{s}(p) = \frac{1}{3} - \mathcal{M}_2(E^\star_{2,p})\rho(E^\star_{2,p}) - \int \frac{dp'p'^2}{(2\pi)^2\omega_{p'}}\mathcal{D}^{(u,u)}_\mathsf{s}(p,p')\rho(E^\star_{2,p'})\,, \tag{28}$$

where

$$\rho(E^\star_{2,p}) \equiv -i\frac{J\big(E^{\star 2}_{2,k}/[2m]^2\big)}{16\pi E^\star_{2,k}}\sqrt{E^{\star 2}_{2,p}/4 - m^2}\,, \tag{29}$$

and it is understood that the the $i\sqrt{-x}$ branch is taken for $x < 0$.

As $\mathcal{K}_{3,\mathsf{iso}}$ is consistent with zero in all fits we have considered, the main purpose in keeping track of these quantities is to estimate the propagation of uncertainties into $\mathcal{M}_3$. In particular we note

$$\Delta\mathcal{M}_3^2 = \sum_{\eta,\eta'}[\partial_\eta\mathcal{M}_3]\,C_{\eta\eta'}\,[\partial_{\eta'}\mathcal{M}_3]\,, \tag{30}$$

where $C_{\eta\eta'}$ represents the fit-parameter covariance matrix and the sums run over all inputs to the scattering amplitude, in particular the scattering length a_0 as well as $\mathcal{K}_{3,\mathsf{iso}}$. In the next section we present numerical solutions for $\mathcal{M}_3$ based on the parameters extracted from the finite-volume energies.

4. Solutions for $\mathcal{M}_3$

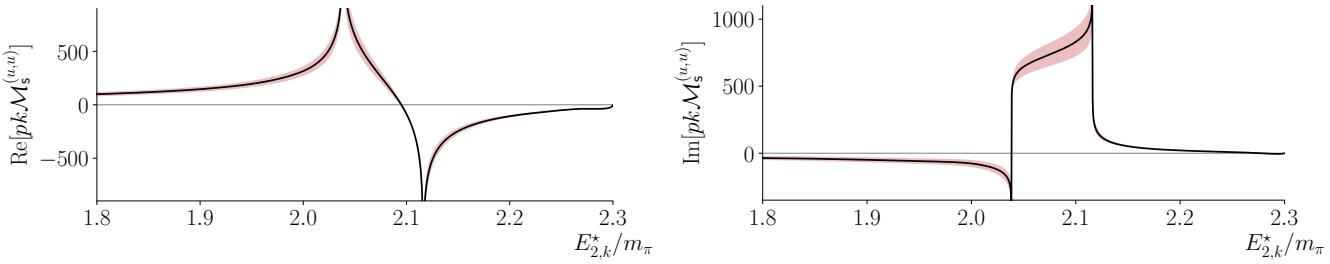

FIG. 4. Real (left) and imaginary (right) parts of $p\,k\,\mathcal{M}_{\mathsf{s}}^{(u,u)}$, determined by solving Eq. (27) using $m_\pi a_0 = 0.296$ and $\mathcal{K}_{3,\mathsf{iso}} = 0$ for the central values. As we explain in the text, the uncertainties here follow from propagating the uncertainties on $\mathcal{K}_{3,\mathsf{iso}}$ and $m_\pi a_0$, taken from Fit B_{2+3} in Table IV.

Figure 4 shows the result of solving Eq. (27) and varying N and ϵ in order to ensure that the ordered double limit has been saturated. Symmetrizing this function over the three incoming and three outgoing momenta yields the full three-hadron scattering amplitude, plotted in Fig. 3 of the main text.

To assign an uncertainty estimate to $\mathcal{M}_{\mathsf{s}}^{(u,u)}(p,k)$ we have applied a straightforward adaptation of Eq. (30). Specializing to the case of only $m_\pi a_0$ and $\mathcal{K}_{3,\mathsf{iso}}$ as input parameters, and neglecting the correlations between them, this becomes

$$\left(\Delta\mathcal{M}_{\mathsf{s}}^{(u,u)}(p,k)\right)^2 = \left(\Delta[m_\pi a_0]\right)^2 \left(\frac{\partial\mathcal{M}_{\mathsf{s}}^{(u,u)}(p,k)}{\partial(m_\pi a_0)}\right)^2 + \left(\Delta\mathcal{K}_{3,\mathsf{iso}}/9\right)^2 + \mathcal{O}(\Delta\mathcal{K}_{3,\mathsf{iso}}\rho\mathcal{M}_2)^2\,, \tag{31}$$

where $\Delta(m_\pi a_0)$ and $\Delta\mathcal{K}_{3,\mathsf{iso}}$ denote the uncertainties on the input parameters and $\Delta\mathcal{M}_{\mathsf{s}}^{(u,u)}(p,k)$ is the resulting amplitude uncertainty plotted in the figure. In practice one finds that $\Delta\mathcal{K}_{3,\mathsf{iso}}$ contributes negligibly to the overall uncertainty, simply because the series of $\mathcal{M}_2$ and G_{s} insertions dominates the value of the amplitude for weakly-interacting systems. For this reason we have taken the leading part of $\mathcal{E}_{\mathsf{s}}^{(u)}$, resulting in the $\Delta\mathcal{K}_{3,\mathsf{iso}}/9$ term. The additional corrections, indicated by the final term, are negligible for this system.

The dominant source of uncertainty enters through the scattering length, i.e. the first term in Eq. (31). To estimate this, we have numerically performed the derivative with respect to $m_\pi a_0$. Since $\mathcal{M}_{\mathsf{s}}^{(u,u)}(p,k)$ is dominated by the contribution proportional to $\mathcal{M}_2^2$, in this case the overall uncertainty is well approximated by

$$\frac{\Delta\mathcal{M}_{\mathsf{s}}^{(u,u)}(p,k)}{\mathcal{M}_{\mathsf{s}}^{(u,u)}(p,k)} = 2\frac{\Delta[m_\pi a_0]}{m_\pi a_0}\,. \tag{32}$$

To produce Fig. 4 we have used $\Delta[m_\pi a_0] = 0.016$ and $\Delta\mathcal{K}_{3,\mathsf{iso}} = 770$. These are taken from B_{2+3} in Table IV with the uncertainty on $m_\pi a_0$ doubled to account for systematic variations between the various fits that have been performed.

5. Operator construction and lists

Following Ref. [1], to determine the $\pi\pi$ $I = 2$ finite-volume energies we compute correlation functions featuring operators constructed to resemble a $\pi\pi$ structure. Schematically, for an operator in lattice irrep Λ_{12} and row μ_{12} with overall momentum $\boldsymbol{k_{12}}$,

$$(\pi\pi)^{[\boldsymbol{k_1},\boldsymbol{k_2}]\dagger}_{\Lambda_{12}\,\mu_{12}}(\boldsymbol{k_{12}}) = \sum_{\substack{\boldsymbol{k_1},\,\boldsymbol{k_2}\\ \boldsymbol{k_1}+\boldsymbol{k_2}=\boldsymbol{k_{12}}}} \mathcal{C}(\boldsymbol{k_{12}},\Lambda_{12},\mu_{12};\boldsymbol{k_1},\Lambda_1;\boldsymbol{k_2},\Lambda_2)\;\pi^\dagger_{\Lambda_1}(\boldsymbol{k_1})\;\pi^\dagger_{\Lambda_2}(\boldsymbol{k_2})\,, \tag{33}$$

where the sum is over all momenta related to $\boldsymbol{k_1}$ and $\boldsymbol{k_2}$ by allowed lattice rotations, $\mathcal{C}$ is an appropriate generalized Clebsch-Gordan coefficient for $\Lambda_1 \otimes \Lambda_2 \to \Lambda_{12}$, and flavor indices and the projection onto $I = 2$ are not written explicitly. Here $\pi^\dagger_{\Lambda_i}(\boldsymbol{k_i})$ is the optimal linear combination of operators to interpolate a π with momentum $\boldsymbol{k_i}$ in irrep[1]

[1] These are all one dimensional and so we omit the irrep row index.

$\boldsymbol{P}$ Λ	$L/a_s = 20$	$L/a_s = 24$
[000] A_1^+	$\pi_{[000]}\pi_{[000]}$, $\pi_{[100]}\pi_{[100]}$, $\pi_{[110]}\pi_{[110]}$, $\pi_{[111]}\pi_{[111]}$, $\pi_{[200]}\pi_{[200]}$	$\pi_{[000]}\pi_{[000]}$, $\pi_{[100]}\pi_{[100]}$, $\pi_{[110]}\pi_{[110]}$, $\pi_{[111]}\pi_{[111]}$, $\pi_{[200]}\pi_{[200]}$
[100] A_1	$\pi_{[000]}\pi_{[100]}$, $\pi_{[100]}\pi_{[110]}$, $\pi_{[110]}\pi_{[111]}$, $\pi_{[100]}\pi_{[200]}$	$\pi_{[000]}\pi_{[100]}$, $\pi_{[100]}\pi_{[110]}$, $\pi_{[110]}\pi_{[111]}$, $\pi_{[100]}\pi_{[200]}$, $\pi_{[110]}\pi_{[210]}$, $\pi_{[200]}\pi_{[210]}$, $\pi_{[111]}\pi_{[211]}$
[110] A_1	$\pi_{[000]}\pi_{[110]}$, $\pi_{[100]}\pi_{[100]}$, $\pi_{[100]}\pi_{[111]}$, $\pi_{[110]}\pi_{[110]}$	$\pi_{[000]}\pi_{[110]}$, $\pi_{[100]}\pi_{[100]}$, $\pi_{[100]}\pi_{[111]}$, $\pi_{[110]}\pi_{[110]}$, $\pi_{[110]}\pi_{[200]}$, $\pi_{[100]}\pi_{[210]}$, $\pi_{[111]}\pi_{[210]}$, $\pi_{[110]}\pi_{[211]}$
[111] A_1	$\pi_{[000]}\pi_{[111]}$, $\pi_{[100]}\pi_{[110]}$	$\pi_{[000]}\pi_{[111]}$, $\pi_{[100]}\pi_{[110]}$, $\pi_{[111]}\pi_{[200]}$, $\pi_{[110]}\pi_{[210]}$, $\pi_{[100]}\pi_{[211]}$
[200] A_1	$\pi_{[100]}\pi_{[100]}$, $\pi_{[000]}\pi_{[200]}$, $\pi_{[110]}\pi_{[110]}$, $\pi_{[111]}\pi_{[111]}$	$\pi_{[100]}\pi_{[100]}$, $\pi_{[000]}\pi_{[200]}$, $\pi_{[110]}\pi_{[110]}$, $\pi_{[100]}\pi_{[210]}$, $\pi_{[111]}\pi_{[111]}$, $\pi_{[110]}\pi_{[211]}$, $\pi_{[210]}\pi_{[210]}$

TABLE V. The $\pi\pi$ $I = 2$ operators, $\pi_{\boldsymbol{k_1}}\pi_{\boldsymbol{k_2}}$, used to compute the finite-volume energy levels shown in Fig. 1 of the main text (upper plots) in irrep Λ with overall momentum $\boldsymbol{P}$. These are constructed from optimized π operators with momentum types $\boldsymbol{k_1}$ and $\boldsymbol{k_2}$; different momentum directions are summed over as in Eq. (33). Momenta are displayed using the shorthand notation $[ijk] = \frac{2\pi}{L}(i, j, k)$.

Λ_i using a basis of fermion-bilinear operators featuring various Dirac γ matrices and gauge-covariant derivatives – see Ref. [1] for details. In this work the basis of fermion-bilinear operators used for a π operator has up to three derivatives for π at rest and up to one derivative for π at non-zero momentum, except we use up to two derivatives for $1 \leq |\boldsymbol{k_i}|^2 \leq 4$ on the 24^3 volume. The operators used to compute the $\pi\pi$ spectra shown in Fig. 1 of the main text are listed in Table V.

In a similar way, operators used to compute $\pi\pi\pi$ $I = 3$ energies resemble a $\pi\pi\pi$ structure and are formed by combining a $\pi\pi$ $I = 2$ operator with a π operator, as detailed in Ref. [5]. Schematically, for an operator in lattice irrep Λ and row μ with overall momentum $\boldsymbol{P}$,

$$(\pi\pi\pi)^{[\boldsymbol{k_{12}}[\boldsymbol{k_1},\boldsymbol{k_2}],\boldsymbol{k_3}]\dagger}_{\Lambda\,\mu}(\boldsymbol{P}) = \sum_{\substack{\boldsymbol{k_{12}},\,\boldsymbol{k_3} \\ \boldsymbol{k_{12}}+\boldsymbol{k_3}=\boldsymbol{P}}} \mathcal{C}(\boldsymbol{P},\Lambda,\mu;\boldsymbol{k_{12}},\Lambda_{12},\mu_{12};\boldsymbol{k_3},\Lambda_3)\,(\pi\pi)^{[\boldsymbol{k_1},\boldsymbol{k_2}]\dagger}_{\Lambda_{12}\,\mu_{12}}(\boldsymbol{k_{12}})\,\pi^\dagger_{\Lambda_3}(\boldsymbol{k_3})\,, \tag{34}$$

where the sum is over all momenta related to $\boldsymbol{k_{12}}$ and $\boldsymbol{k_3}$ by allowed lattice rotations and, again, flavor indices and the projection onto $I = 3$ are not written explicitly.

From Bose symmetry, a $\pi\pi\pi$ system must be symmetric under the interchange of any pair of pions. The pions have no intrinsic spin and we are considering $I = 3$ which means that the flavor structure is symmetric under interchange of any pair; therefore, the spatial structure must also be symmetric under the interchange of any pair of pions. The operator construction in Eq. (34) gives operators with the correct symmetry properties because the three pions are identical, but it does not make this symmetry manifest and two different sets of ($|\boldsymbol{k_1}|$, $|\boldsymbol{k_2}|$, $|\boldsymbol{k_3}|$, $|\boldsymbol{k_{12}}|$, Λ_{12}) may lead to equivalent operators, or a number of different sets may give linearly-dependent operators.[2] To ensure we have an appropriate set of independent operators, for each $\boldsymbol{P}$ and Λ, we construct an operator for every possible set ($|\boldsymbol{k_1}|$, $|\boldsymbol{k_2}|$, $|\boldsymbol{k_3}|$, $|\boldsymbol{k_{12}}|$, Λ_{12}) with $|\boldsymbol{k_1}|^2 + |\boldsymbol{k_2}|^2 + |\boldsymbol{k_3}|^2$ less than some cutoff. We write Eq. (34) schematically as,

$$(\pi\pi\pi)_{\Lambda\mu}(\boldsymbol{P}) = \sum \widetilde{\mathcal{C}}(\boldsymbol{k_1},\boldsymbol{k_2},\boldsymbol{k_3})\,\pi^\dagger(\boldsymbol{k_1})\pi^\dagger(\boldsymbol{k_2})\pi^\dagger(\boldsymbol{k_3}) = \widetilde{\mathcal{C}}\cdot\mathcal{V}_{[\pi\pi\pi]}\,, \tag{35}$$

where $\widetilde{\mathcal{C}}$ with no labels represents a row vector of coefficients and $\mathcal{V}_{[\pi\pi\pi]}$ a column of operators, such that the dot-product reproduces the sum. We then introduce the matrix $R(ijk)$ which acts on $\mathcal{V}_{[\pi\pi\pi]}$ by mapping a given entry $\pi^\dagger(\boldsymbol{p}_1)\pi^\dagger(\boldsymbol{p}_2)\pi^\dagger(\boldsymbol{p}_3)$ into $\pi^\dagger(\boldsymbol{p}_i)\pi^\dagger(\boldsymbol{p}_j)\pi^\dagger(\boldsymbol{p}_k)$. This allows us to define the symmetrized vector of Clebsch-Gordan coefficients

$$\widetilde{\mathcal{C}}\cdot R(123) + \widetilde{\mathcal{C}}\cdot R(231) + \widetilde{\mathcal{C}}\cdot R(312) + \widetilde{\mathcal{C}}\cdot R(132) + \widetilde{\mathcal{C}}\cdot R(213) + \widetilde{\mathcal{C}}\cdot R(321)\,, \tag{36}$$

[2] Strictly we mean the types of momenta (i.e. the equivalence class of momenta related by rotations in the octahedral group or little group) rather than the magnitudes, but there is no distinction for the momenta we are considering here.

where $R(123)$ is just the identity matrix. The final step is to check that the resulting vector is non-zero and linearly independent from the analogous expressions for the already considered operators. The resulting sets of independent operators used in this work are listed in Tables VI, VII, VIII, IX and X.[3]

Finally, in order to give further intuition into the operators used, we also include a diagrammatic representation of the individual pion momentum assignments in the tables. The diagrams portray the integer vectors $\boldsymbol{d}_1$, $\boldsymbol{d}_2$, $\boldsymbol{d}_3$, each given by $\boldsymbol{d}_i = L\boldsymbol{k}_i/(2\pi)$. The vectors are assigned a color (orange and green for the first two pions, and blue for the third) and the absence of any given color corresponds to a vector of magnitude zero. As summarized by Eq. (34), our operator construction is based on combining two-pion operators in a definite irrep with the third pion. An alternative basis is given by summing a given momentum assignment, represented by a given set $\boldsymbol{d}_1\boldsymbol{d}_2\boldsymbol{d}_3$, over all rotations in the octahedral group (in the case of $\boldsymbol{P} = [000]$) or else a little group thereof (for non-zero total momentum) weighted by the appropriate Clebsch-Gordan coefficients. The operators reached via this alternative construction are equal to a linear combination of those given by Eq. (34).

For example, on the third line of Table VII, two distinct momentum assignments arise from combining the $\pi\pi_{[000]A_1^+}$ with the third $\pi_{[100]}$ operator. In this case the $\pi\pi_{[000]A_1^+}$ is built from individual pions with a unit of back-to-back momentum. When one sums over the coefficients projecting onto A_1^+, contributions arise with the back-to-back axis both aligned and perpendicular to the total momentum direction, $\boldsymbol{P} = [001]$. Thus, momentum assignments corresponding to both diagrams shown in line 3 of Table VII contribute to the operator on that line. By contrast, on line 4 of Table VII only a single momentum configuration contributes, as indicated. This implies that the two operators are independent, since they are built from independent linear combinations of the two momentum configurations.

Operators 8 through 11 of Table VII give a more complicated example. The first two (8 and 9) correspond to two linear combinations of two configuration types, labeled with subscripts 1 and 3, and the next two (10 and 11) are equal to linear combinations of the operators labeled 1, 2, and 4.

The diagrams in Tables VI, VII, VIII, IX and X provide a cross check on the linear-independence of the operators. Each row corresponds to a linear combination of the displayed momentum configurations and the number of linearly independent operators is equal to the number of distinct diagrams.

[1] J. J. Dudek, R. G. Edwards, and C. E. Thomas, Phys. Rev. **D86**, 034031 (2012), arXiv:1203.6041 [hep-ph].
[2] M. T. Hansen and S. R. Sharpe, Phys. Rev. **D90**, 116003 (2014), arXiv:1408.5933 [hep-lat].
[3] M. T. Hansen and S. R. Sharpe, Phys. Rev. **D92**, 114509 (2015), arXiv:1504.04248 [hep-lat].
[4] A. Jackura, C. Fernández-Ramírez, V. Mathieu, M. Mikhasenko, J. Nys, A. Pilloni, K. Saldaña, N. Sherrill, and A. P. Szczepaniak (JPAC), Eur. Phys. J. **C79**, 56 (2019), arXiv:1809.10523 [hep-ph].
[5] A. J. Woss, C. E. Thomas, J. J. Dudek, R. G. Edwards, and D. J. Wilson, Phys. Rev. **D100**, 054506 (2019), arXiv:1904.04136 [hep-lat].

[3] This is not always a unique choice and any independent set of operators could be used to achieve the same results.

	$\boldsymbol{d_1^2\, d_2^2\, d_3^2}$	$\pi_{\boldsymbol{k_1}}$	$\pi_{\boldsymbol{k_2}}$	$\pi\pi_{\boldsymbol{k_{12}}\Lambda_{12}}$ $(I=2)$	$\pi_{\boldsymbol{k_3}}$	momentum configurations
1	**000**	$\pi_{[000]}$	$\pi_{[000]}$	$\pi\pi_{[000]A_1^+}$	$\pi_{[000]}$	
2	**011**	$\pi_{[100]}$	$\pi_{[000]}$	$\pi\pi_{[100]A_1}$	$\pi_{[100]}$	
3	**022**	$\pi_{[110]}$	$\pi_{[000]}$	$\pi\pi_{[110]A_1}$	$\pi_{[110]}$	
4	**112**	$\pi_{[100]}$	$\pi_{[100]}$	$\pi\pi_{[110]A_1}$	$\pi_{[110]}$	
5	**033**	$\pi_{[111]}$	$\pi_{[111]}$	$\pi\pi_{[000]A_1^+}$	$\pi_{[000]}$	
6	**114**	$\pi_{[200]}$	$\pi_{[100]}$	$\pi\pi_{[100]A_1}$	$\pi_{[100]}$	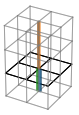
7	**123**	$\pi_{[111]}$	$\pi_{[100]}$	$\pi\pi_{[110]A_1}$	$\pi_{[110]}$	
8	**222**	$\pi_{[110]}$	$\pi_{[110]}$	$\pi\pi_{[110]A_1}$	$\pi_{[110]}$	
9	**044**	$\pi_{[200]}$	$\pi_{[000]}$	$\pi\pi_{[200]A_1}$	$\pi_{[200]}$	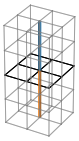
10	**125**	$\pi_{[210]}$	$\pi_{[100]}$	$\pi\pi_{[110]A_1}$	$\pi_{[110]}$	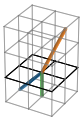

TABLE VI. The $\pi\pi\pi$ $I=3$ operators used to compute the finite-volume energy levels shown in Fig. 1 of the main text (lower left plot) in irrep A_1^- with overall momentum $\boldsymbol{P}=[000]$, labeled by $\boldsymbol{d}_1^2\,\boldsymbol{d}_2^2\,\boldsymbol{d}_3^2$ where $\boldsymbol{d_i}=\boldsymbol{k_i}(L/2\pi)$. Different momentum directions for the momentum types $\boldsymbol{k_1}$, $\boldsymbol{k_2}$, $\boldsymbol{k_3}$ and $\boldsymbol{k_{12}}$ are summed over as in Eq. (34). Operators 1 to 8 are used on the 20^3 volume and operators 1 to 10 are used on the 24^3 volume. The momentum configuration diagrams in the rightmost column are explained in the text. Operators separated by a single horizontal line correspond to states that are degenerate in the non-relativistic, non-interacting theory.

	$d_1^2\, d_2^2\, d_3^2$	$\pi_{\boldsymbol{k_1}}$	$\pi_{\boldsymbol{k_2}}$	$\pi\pi_{\boldsymbol{k_{12}}\Lambda_{12}}$ $(I=2)$	$\pi_{\boldsymbol{k_3}}$	momentum configurations
1	**001**	$\pi_{[000]}$	$\pi_{[000]}$	$\pi\pi_{[000]A_1^+}$	$\pi_{[100]}$	
2	**012**	$\pi_{[100]}$	$\pi_{[000]}$	$\pi\pi_{[100]A_1}$	$\pi_{[110]}$	
3	**111**	$\pi_{[100]}$	$\pi_{[100]}$	$\pi\pi_{[000]A_1^+}$	$\pi_{[100]}$	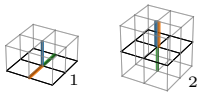
4	**111**	$\pi_{[100]}$	$\pi_{[100]}$	$\pi\pi_{[110]A_1}$	$\pi_{[100]}$	
5	**014**	$\pi_{[100]}$	$\pi_{[000]}$	$\pi\pi_{[100]A_1}$	$\pi_{[200]}$	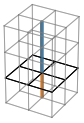
6	**023**	$\pi_{[110]}$	$\pi_{[000]}$	$\pi\pi_{[110]A_1}$	$\pi_{[111]}$	
7	**113**	$\pi_{[100]}$	$\pi_{[100]}$	$\pi\pi_{[110]A_1}$	$\pi_{[111]}$	
8	**122**	$\pi_{[110]}$	$\pi_{[100]}$	$\pi\pi_{[111]A_1}$	$\pi_{[110]}$	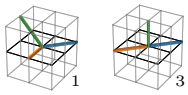
9	**122**	$\pi_{[110]}$	$\pi_{[100]}$	$\pi\pi_{[111]E_2}$	$\pi_{[110]}$	
10	**122**	$\pi_{[110]}$	$\pi_{[100]}$	$\pi\pi_{[100]A_1}$	$\pi_{[110]}$	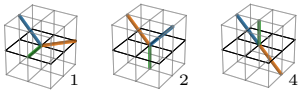
11	**122**	$\pi_{[110]}$	$\pi_{[100]}$	$\pi\pi_{[100]B_1}$	$\pi_{[110]}$	
12	**025**	$\pi_{[110]}$	$\pi_{[000]}$	$\pi\pi_{[110]A_1}$	$\pi_{[210]}$	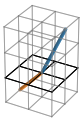
13	**115**	$\pi_{[210]}$	$\pi_{[100]}$	$\pi\pi_{[110]A_1}$	$\pi_{[100]}$	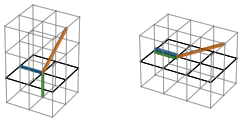
14	**115**	$\pi_{[210]}$	$\pi_{[100]}$	$\pi\pi_{[110]B_1}$	$\pi_{[100]}$	
15	**124**	$\pi_{[200]}$	$\pi_{[100]}$	$\pi\pi_{[210]A_1}$	$\pi_{[110]}$	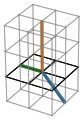
16	**124**	$\pi_{[200]}$	$\pi_{[100]}$	$\pi\pi_{[100]A_1}$	$\pi_{[110]}$	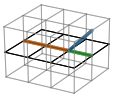

TABLE VII. As Table VI but for the A_2 irrep with overall momentum $\boldsymbol{P} = [001]$. Operators 1 to 8 are used on the 20^3 volume and operators 1 to 16 are used on the 24^3 volume. Operators separated by a single horizontal line correspond to states that are degenerate in the non-relativistic, non-interacting theory. Operators with no horizontal line correspond to states that are degenerate in the relativistic, non-interacting theory but are split by the interactions.

	$\boldsymbol{d_1^2\, d_2^2\, d_3^2}$	$\pi_{\boldsymbol{k_1}}$	$\pi_{\boldsymbol{k_2}}$	$\pi\pi_{\boldsymbol{k_{12}}\Lambda_{12}}$ $(I=2)$	$\pi_{\boldsymbol{k_3}}$	momentum configurations
1	**002**	$\pi_{[000]}$	$\pi_{[000]}$	$\pi\pi_{[000]A_1^+}$	$\pi_{[110]}$	
2	**011**	$\pi_{[100]}$	$\pi_{[000]}$	$\pi\pi_{[100]A_1}$	$\pi_{[100]}$	
3	**013**	$\pi_{[100]}$	$\pi_{[000]}$	$\pi\pi_{[100]A_1}$	$\pi_{[111]}$	
4	**022**	$\pi_{[110]}$	$\pi_{[000]}$	$\pi\pi_{[110]A_1}$	$\pi_{[110]}$	
5	**112**	$\pi_{[100]}$	$\pi_{[100]}$	$\pi\pi_{[000]A_1^+}$	$\pi_{[110]}$	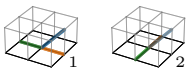
6	**112**	$\pi_{[100]}$	$\pi_{[100]}$	$\pi\pi_{[110]A_1}$	$\pi_{[110]}$	
7	**112**	$\pi_{[100]}$	$\pi_{[100]}$	$\pi\pi_{[200]A_1}$	$\pi_{[110]}$	
8	**112**	$\pi_{[100]}$	$\pi_{[100]}$	$\pi\pi_{[000]E^+}$	$\pi_{[110]}$	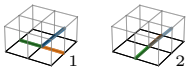

TABLE VIII. As Table VI but for the A_2 irrep with overall momentum $\boldsymbol{P} = [011]$ (continued in Table IX). Operators 1 to 11 are used on the 20^3 volume and operators 1 to 20 are used on the 24^3 volume.

	$\boldsymbol{d_1^2\, d_2^2\, d_3^2}$	$\pi_{\boldsymbol{k_1}}$	$\pi_{\boldsymbol{k_2}}$	$\pi\pi_{\boldsymbol{k_{12}}\Lambda_{12}}$ $(I=2)$	$\pi_{\boldsymbol{k_3}}$	momentum configurations
9	**015**	$\pi_{[100]}$	$\pi_{[000]}$	$\pi\pi_{[100]A_1}$	$\pi_{[210]}$	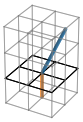
10	**024**	$\pi_{[110]}$	$\pi_{[000]}$	$\pi\pi_{[110]A_1}$	$\pi_{[200]}$	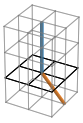
11	**114**	$\pi_{[200]}$	$\pi_{[100]}$	$\pi\pi_{[210]A_1}$	$\pi_{[100]}$	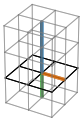
12	**123**	$\pi_{[111]}$	$\pi_{[100]}$	$\pi\pi_{[211]A_1}$	$\pi_{[110]}$	
13	**123**	$\pi_{[111]}$	$\pi_{[100]}$	$\pi\pi_{[110]A_1}$	$\pi_{[110]}$	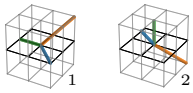
14	**123**	$\pi_{[111]}$	$\pi_{[100]}$	$\pi\pi_{[110]B_2}$	$\pi_{[110]}$	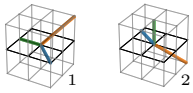
15	**222**	$\pi_{[110]}$	$\pi_{[110]}$	$\pi\pi_{[000]A_1^+}$	$\pi_{[110]}$	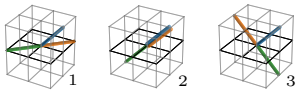
16	**222**	$\pi_{[110]}$	$\pi_{[110]}$	$\pi\pi_{[211]A_1}$	$\pi_{[110]}$	
17	**222**	$\pi_{[110]}$	$\pi_{[110]}$	$\pi\pi_{[110]A_1}$	$\pi_{[110]}$	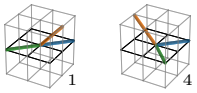
18	**222**	$\pi_{[110]}$	$\pi_{[110]}$	$\pi\pi_{[200]A_1}$	$\pi_{[110]}$	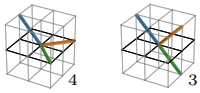
19	**026**	$\pi_{[110]}$	$\pi_{[000]}$	$\pi\pi_{[110]A_1}$	$\pi_{[211]}$	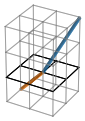
20	**035**	$\pi_{[111]}$	$\pi_{[000]}$	$\pi\pi_{[111]A_1}$	$\pi_{[210]}$	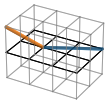

TABLE IX. Continuation of Table VIII.

	$\boldsymbol{d_1^2\, d_2^2\, d_3^2}$	$\pi_{\boldsymbol{k_1}}$	$\pi_{\boldsymbol{k_2}}$	$\pi\pi_{\boldsymbol{k_{12}}\Lambda_{12}}$ $(I=2)$	$\pi_{\boldsymbol{k_3}}$	momentum configurations
1	**003**	$\pi_{[000]}$	$\pi_{[000]}$	$\pi\pi_{[000]A_1^+}$	$\pi_{[111]}$	
2	**012**	$\pi_{[110]}$	$\pi_{[000]}$	$\pi\pi_{[110]A_1}$	$\pi_{[100]}$	
3	**111**	$\pi_{[100]}$	$\pi_{[100]}$	$\pi\pi_{[110]A_1}$	$\pi_{[100]}$	
4	**113**	$\pi_{[100]}$	$\pi_{[100]}$	$\pi\pi_{[000]A_1^+}$	$\pi_{[111]}$	
5	**113**	$\pi_{[100]}$	$\pi_{[100]}$	$\pi\pi_{[200]A_1}$	$\pi_{[111]}$	
6	**122**	$\pi_{[110]}$	$\pi_{[100]}$	$\pi\pi_{[100]A_1}$	$\pi_{[110]}$	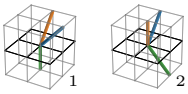
7	**122**	$\pi_{[110]}$	$\pi_{[110]}$	$\pi\pi_{[110]A_1}$	$\pi_{[100]}$	

TABLE X. As Table VI but for the A_2 irrep with overall momentum $\boldsymbol{P} = [111]$. Operators 1 to 7 are used on both the 20^3 and 24^3 volumes.